RSC Advances

PAPER

View Article Online
View Journal | View Issue

Cite this: *RSC Adv.*, 2016, **6**, 13286

Solvent compatible microfluidic platforms for pharmaceutical solid form screening†

Sachit Goyal,[ab] Aristotle E. Economou,‡[b] Theodore Papadopoulos,‡[b] Elizabeth M. Horstman,[b] Geoff G. Z. Zhang,[c] Yuchuan Gong*[c] and Paul J. A. Kenis*[b]

We describe a microfluidic platform with enhanced solvent compatibility to screen solid forms of pharmaceutical parent compounds including salts, cocrystals, and their crystal forms *via* controlled solvent evaporation and antisolvent addition techniques. The platform enables on-chip combinatorial mixing of parent compound, auxiliary materials, or non-solvents in a 24- to 72-well array (~100–200 nL per well). This approach enables screening with very small quantities of material per condition compared to traditional screening approaches that require larger volumes, ~100 μL per well. Compatibility with (i) polar as well as non-polar organic solvents commonly employed in crystallization of pharmaceuticals, such as ethanol, methanol, tetrahydrofuran, acetonitrile, chloroform, hexane, and toluene, (ii) Raman spectroscopy used for on-line identification of the resulting solids was achieved by using a perfluoropolyether-based microfluidic platform. Integration of a hybrid thin layer assembly of elastomeric PDMS–SIFEL–SIFEL ensures that pneumatic valving capabilities are retained. This assembly was sandwiched between layers of cyclic-olefin copolymer (COC) at the top and Teflon FEP or COC (depending on the solvent) at the bottom to yield a physically rigid, Raman compatible crystallization chip. In addition, a solvent-impermeable thiolene layer patterned with evaporation channels was employed to permit control over the rate of solvent evaporation for solvent evaporation experiments. The resulting hybrid microfluidic platforms enabled enhanced compatibility with a variety of polar and non-polar organic solvents such as methanol, ethanol, isopropyl alcohol, acetonitrile, tetrahydrofuran, hexane, heptane, and toluene, which is especially critical for antisolvent crystallization experiments. In solvent evaporation experiments with these platforms the rate of solvent evaporation can be controlled consistently (5–20 nL h^{-1}), thereby facilitating nucleation and crystal growth. Model compounds, theophylline and carbamazepine, were used to validate the platform's ability to screen for cocrystals *via* solvent evaporation and for polymorphs *via* antisolvent addition. On-chip Raman analysis was used to identify different cocrystals and polymorphs.

Received 10th December 2015
Accepted 12th January 2016

DOI: 10.1039/c5ra26426j

www.rsc.org/advances

Introduction

Solid form screening is an integral process in pharmaceutical development which involves crystallization under a wide range of conditions such as, active pharmaceutical ingredient (APIs)/small molecule ratios, temperature, solvent/antisolvent ratios, and pH. These crystallization conditions are used to identify possible solid forms (*e.g.* salts, cocrystals, polymorphs, hydrates) and elucidate different crystal habits. Crystal habit (shape/size) affects drug processing and the dissolution rate of APIs.[1,2] Current methods for solid form screening often involve use of automated tools to increase throughput, thus reducing turnaround time compared to manual screening methods. However, these robotic tools typically require ~0.5 g of the API for a screen involving 100 experiments, quantities that typically are not available in the early stages of drug discovery. Hence, solid form screening is initiated late in the drug discovery process when a gram or more of the API is available.[3–6] Microfluidic approaches can enable solid form screening of APIs utilizing much smaller amounts of materials, *i.e.*, on the order of 0.5 mg for a 100-experiment screen, thereby enabling extensive solid form screening with limited amount of API available in the earlier stages of drug development.[5,6]

Progress in microfluidics over the last few decades has resulted in the development of microfluidic platforms for a wide

[a]*The Dow Chemical Company, Polyurethanes R&D, 2301 North Brazosport Boulevard B 1680 #221, Freeport, Texas, 77541, USA*

[b]*Department of Chemical & Biomolecular Engineering, University of Illinois at Urbana-Champaign, 600 South Mathews Avenue, Urbana, Illinois 61801, USA. E-mail: kenis@illinois.edu; Tel: +1 217 265 0523*

[c]*Drug Product Development, Research and Development, AbbVie Inc., 1 N Waukegan Road, North Chicago, Illinois 60064, USA. E-mail: yuchuan.gong@abbvie.com; Tel: +1 847 938 6642*

† Electronic supplementary information (ESI) available. See DOI: 10.1039/c5ra26426j

‡ Authors contributed equally to the work.

range of biological applications, for example: gene expression,[7] single cell analysis,[8] digital PCR,[9] DNA sequencing,[10] and analysis,[11] and point-of-care and clinical diagnostics.[12–14] Furthermore, microfluidic platforms have been developed for protein and pharmaceuticals crystallization.[15–31] Examples include free interface diffusion (FID) based platforms,[15,32] droplet based microfluidics,[25,33–37] evaporation-based platforms,[18,38] and slip-chip approaches.[22,24,39] Similarly, microfluidic platforms for pharmaceutical crystallization have been developed to screen for different solid forms of APIs such as salts, polymorphs, and cocrystals[38,40–47] to allow for solid form screening at earlier stages of drug development when only very small quantities of API are available. For example, platforms based on droplets,[43,45] patterned surfaces,[46] free interface diffusion,[41,42] antisolvent addition,[40] temperature control,[44] and evaporation[38] have been employed for pharmaceutical crystallization. Some of the aforementioned platforms allow for crystal harvesting and subsequent analysis *via* traditional approaches (*e.g.*, Raman spectroscopy, X-ray diffraction).[16,25,29] In contrast, some platforms have been reported that enable on-chip analysis of the solid forms, obviating the need to manually handle crystals.[15,26,38,40–42,48–50] Droplet and slip-chip based microfluidic tools enable high-throughput screening of crystallization conditions but lack desirable charactreistics; for example the PDMS-based droplet-based tools[33,37,51] lack the compatibility with organic solvents and slip-chip based tools[23] do not allow on-chip solid form analysis.

Previously, we reported on multilayer microfluidic platforms comprised of poly-dimethylsiloxane (PDMS) and cyclic olefin copolymer (COC) as well as PDMS–COC–thiolene. Key features of these devices are the combinatorial mixing capabilities enabling high throughput screening (50–200 nL sample volume per well) and the compatibility with on-chip solid form analysis *via* optical microscopy, Raman spectroscopy, and/or X-ray diffraction.[15,52] The reported platforms were engineered to ensure compatibility with some of the commonly used polar organic solvents employed in pharmaceutical crystallization, including alcohols, water, acetonitrile, and DMSO. These platforms were employed to screen a wide range of crystallization conditions for pharmaceutical solid forms including salts,[41] cocrystals,[42,47] and polymorphs[40] employing free-interface diffusion (FID),[41] antisolvent addition,[40] and solvent evaporation[38] modes of crystallization.

A large proportion of new pharmaceutically active entities being developed in the pharmaceutical industry have high molecular weight (MW ranging for 800–1600 g mol^{-1}) and consequently are poorly soluble in aqueous media.[53] These pharmaceutically active entities typically require strong organic solvents (*e.g.*, chloroform, tertrahydrofuran (THF), ethyl acetate, DMSO) to solubilize the drug and enable subsequent crystallization. PDMS and COC are known to have limited compatibility with most of the stronger polar organic solvents (*e.g.*, THF, ethyl acetate) and non-polar organic solvents (*e.g.*, hexanes, toluene).[54,55] Development of microfluidic platforms with enhanced solvent resistance would enable screening of crystallization conditions in a wider range of solvents that cannot be employed in the previously reported PDMS/COC-based microfluidic platforms.

A broad range of polymeric materials has been explored for microfluidic applications that require compatibility with certain organic solvents, including thiolene,[56–58] untreated fluoropolymers,[59] photo-curable or thermally curable perfluoropolyether,[60–63] polytetrafluoroethylene or Teflon,[64] thermoset polyester,[65,66] cyclic olefin copolymer,[67] Viton,[68] SU-8,[69] parylene,[70] polyimide,[71] polyvinyl(silazane),[72] and Dyneon™ THV Fluorothermoplastics.[73] However, the majority of these polymers suffer from one or more of the following limitations that hamper their use in the development of a high throughput screening platform: (1) incompatibility with a wide range of organic solvents for extended use; (2) complex and cost intensive fabrication (*e.g.*, requiring an oxygen-free environment); (3) non-amenability with rapid prototyping; and (4) incompatibility of on-chip solid form analysis. For example, droplet based microfluidics made of PTFE, glass, and Teflon tubes have been demonstrated to perform with multiple solvents however controlled solvent evaporation platforms using these materials has not been demonstrated.[35,36] Microfluidic platforms with enhanced solvent compatibility that can be fabricated *via* soft lithographic methods, while ensuring high throughput capabilities, portability between stations, and allowing for on-chip solid form analysis *via* X-ray and Raman have the potential to aid solid form screening or other crystallization experiments involving strongly polar as well as non-polar organic solvents.

Here, we report on the development and application of multilayer hybrid-COC/PDMS/SIFEL/COC or Teflon-FEP/thiolene-based solvent compatible microfluidic platforms for solid form screening of APIs, specifically for crystallization screening *via* diffusive mixing, antisolvent addition, and solvent evaporation. The platforms reported here are compatible with a wide range of organic solvents, including ethanol, methanol, THF, acetonitrile, chloroform, hexane, and toluene, and allow for on-chip solid form analysis *via* Raman spectroscopy. The platforms can be fabricated *via* soft lithographic methods. We validated the platform by screening for cocrystals of theophylline and carbamazepine *via* solvent evaporation and different polymorphs of carbamazepine *via* antisolvent addition.

Materials and methods

Chip assembly

Antisolvent chip. Schematic of the platform is shown in Fig. 1. The platform is a four-layer assembly (FLA, ~250 μm thick) consisting of a solvent impermeable top layer, thin PDMS-adhesion layer, fluid metering layer, and fluid mixing layer, as well as a substrate layer (Teflon 50–100 μm thick).

Evaporation chip. Schematic of the platform is shown in Fig. 1. The platform consists a FLA, an interfacial layer (IL, 60–110 μm thick) including substrate (Teflon) and SIFEL elastomeric sealing layer, and an evaporation layer (EL, 2 mm thick). The EL contains the channels that control solvent evaporation rates. The EL was fabricated (*vide infra*) and reversibly bonded to the IL. Then the EL–IL assembly was reversibly bonded to the FLA.

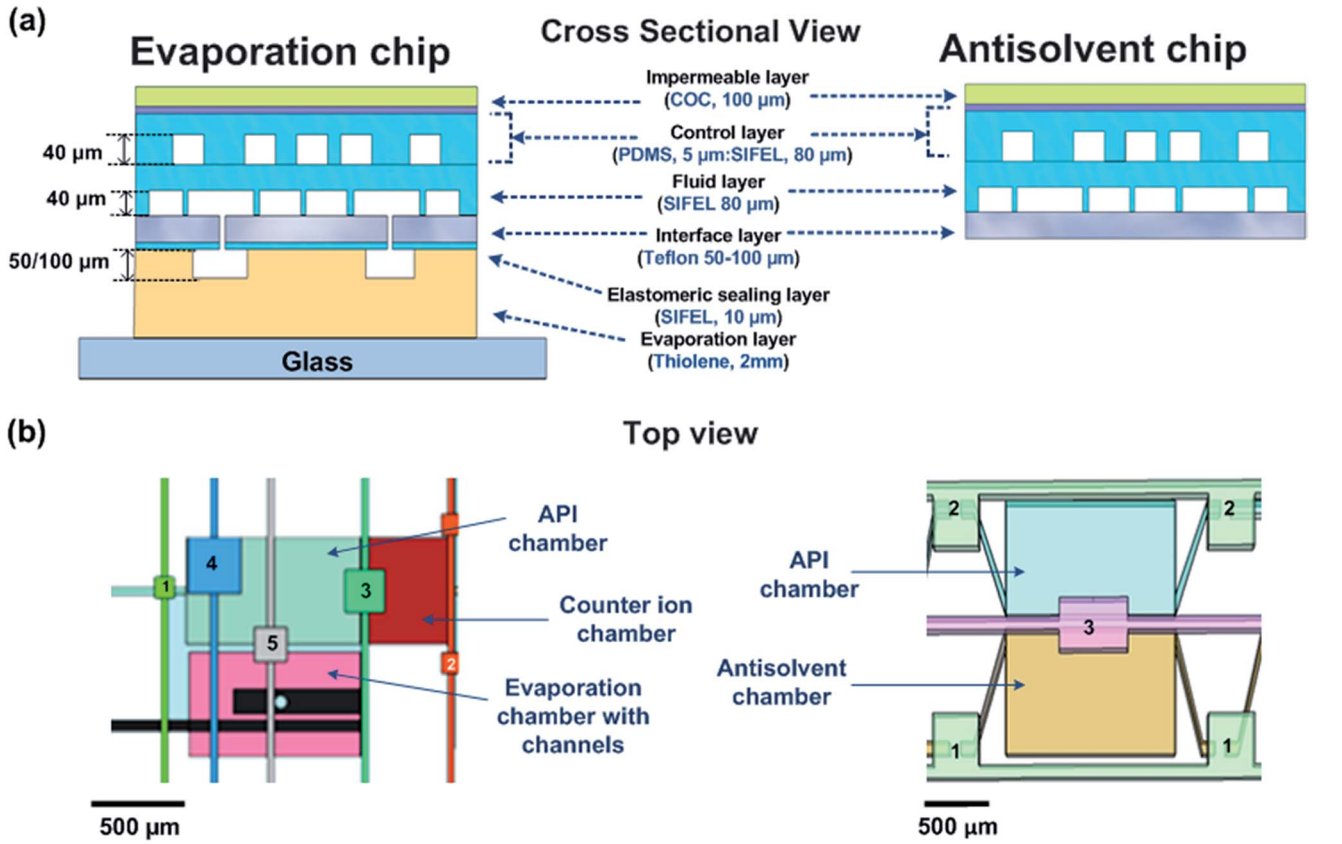

Fig. 1 (a) Cross section of two microfluidic crystallization platforms depicting layered assembly. (b) Top view of the microfluidic platform depicts the control layer aligned over the fluid layer (for the antisolvent-chip), which is further aligned over the evaporation channel layer illustrating the function of different valves in the filling and mixing of solutions on-chip and the evaporation channels in the evaporation of solvents (for the evaporation-chip). The numbers 1–5 refer to different sets of control valves.

Fig. 2 shows detailed views of the assembly of different layers of the chip for evaporation driven crystallization experiment. Details of fabrication procedures for FLA, IL, and EL, as well as chip assembly for evaporation chip are provided in the ESI.†

a. Four-layer assembly (FLA). FLA is comprised of a SIFEL (Shin-Etsu Silicones of America Inc., Part A/B) control layer (CL) and fluid layer (FL), a polydimethylsiloxane (PDMS, General Electric RTV 615, Part A/B) adhesion layer, and a cyclic olefin copolymer (COC) (COC, 6013 grade, TOPAS™ Advanced Polymers) backing layer fabricated as shown in schematic in Fig. 2a.

b. Interfacial layer (IL). IL is comprised of a thin SIFEL layer (5–10 μm) on a Teflon-FEP or AF sheet (50–100 μm) fabricated as shown in the schematic in Fig. 2b.

c. Evaporation layer (EL) fabrication. The EL was fabricated out of NOA–81 thiolene (Norland Products) following procedure established in our previous work.[38] The fabrication process is shown in the schematic in Fig. 2c.

d. Alignment and final assembly of all layers for evaporation chip. First, the IL was placed on the EL and the through-holes connecting the evaporation chambers in the FLA and the corresponding evaporation channels in EL were marked and drilled. Next, the IL was manually aligned and reversibly sealed to the EL. Finally, the FLA was manually aligned and reversible sealed to the IL–EL assembly such that the holes in the evaporation chambers in the FL were aligned with the corresponding evaporation channels. The aligned chip is shown in Fig. 2d.

Preparation of active pharmaceutical ingredient (API) and cocrystal former (CCF) solutions. All APIs and CCFs were obtained from Sigma-Aldrich and used as received.

Polymorph/crystal habit screening. Carbamazepine solutions for polymorph screening were prepared by dissolving carbamazepine in THF (0.5 M), chloroform (0.5 M), and acetonitrile (0.2 M). Hexane and heptane were used as antisolvents.

Cocrystal screening. Solution of theophylline[74] was dissolved in chloroform : ethanol (1 : 1 volumetric ratio) at a concentration of 0.5 M in a glass vial by vortexing (Maxi Mix II, Barnstead/Thermolyne). Four acids (malonic, 2,4-dihydroxy benzoic acid, benzoic acid and glutaric acids) were also dissolved in the same solvent mixture at a concentration of 1.2 M.

Carbamazepine solutions were prepared following the same procedure. Carbamazepine was dissolved in acetonitrile at a concentration of 0.14 M. Acetonitrile solutions of two solid acids (malic acid and 4-hydroxy benzoic acid) were prepared at molar concentration of ~0.30 M.

Crystallization off-chip

Antisolvent addition. Crystallization in the presence of antisolvent was executed in glass vials to obtain reference solids

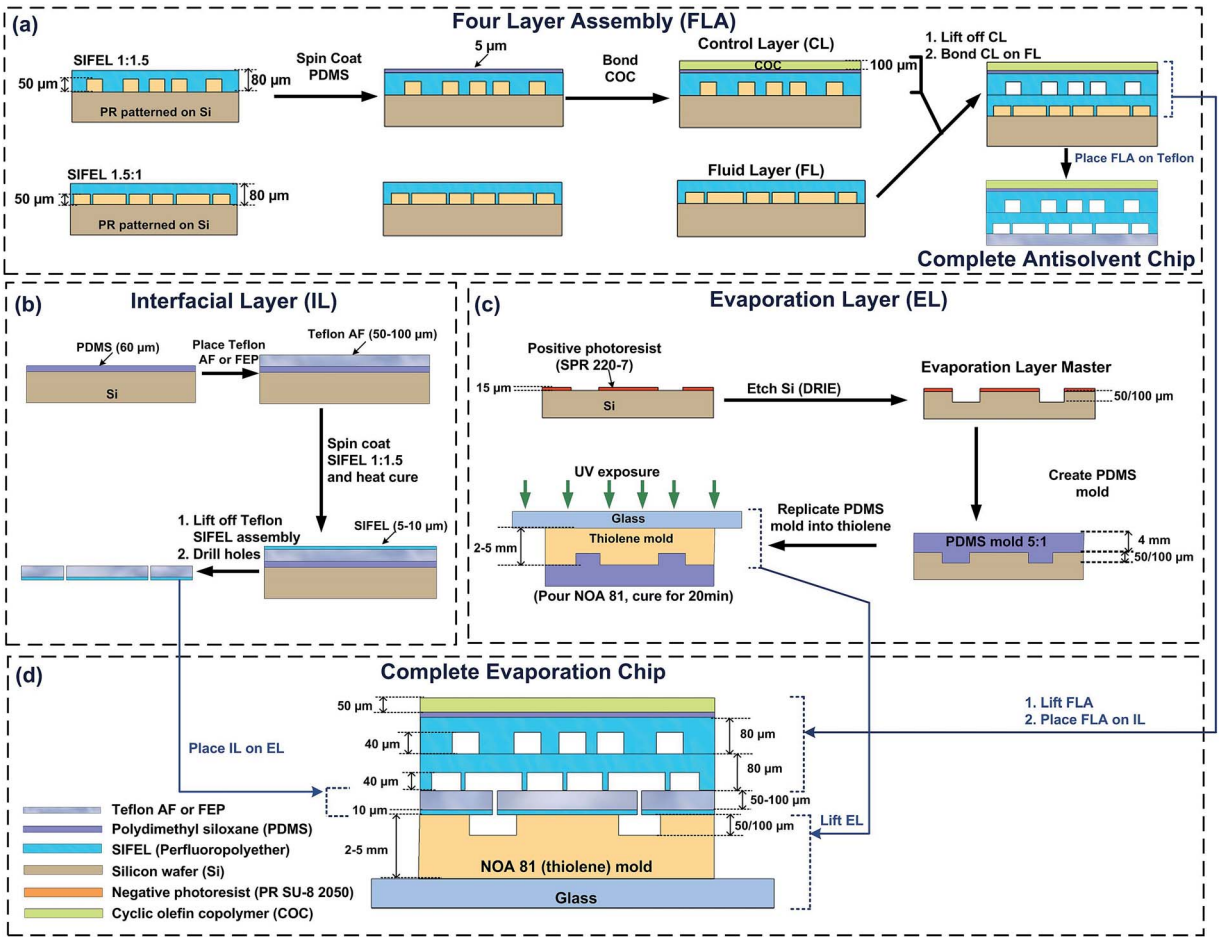

Fig. 2 Fabrication steps for the antisolvent/evaporative chip. (a) Negative patterns for the CL and FL are patterned on Si-wafers, which are replicated in PDMS to obtain the FL and CL, and a COC sheet was irreversibly bonded to the CL spin coated with a thin layer of PDMS enabling adhesion. Then the COC–CL assembly was lifted off the master and sealed with the FL *via* thermal curing to yield the FLA. The FLA was reversibly bonded to a Teflon FEP film or COC film depending on the solvent used to yield the antisolvent chip. (b) The IL is obtained by spin coating and partially curing a thin layer of PDMS on a silanized Si-wafer. A Teflon sheet was placed on the PDMS then a SIFEL layer was spun coat and cured on the surface. Subsequently, this assembly was lifted off from the PDMS coated Si substrate. (c) The EL was created by first creating an appropriate master *via* photolithography and DRIE, followed by replication to obtain a PDMS mold, which in turn is replicated in thiolene by applying the liquid pre-polymer and subsequent UV curing. (d) Chip assembly is completed by placing the IL on the EL, and then placing the FLA on the IL–EL assembly.

for comparison with on-chip crystallization results. The off-chip experiments were conducted in 1 mL glass vials (Kimble/Chase). The effect of antisolvent and solvent type and ratio of antisolvent : solvent mixed on the carbamazepine solids was observed off-chip. Concentrated solutions of carbamazepine were prepared in different solvents (THF, chloroform, and toluene) and mixed with antisolvents (hexane and heptane) in different volumetric ratios (1 : 2, 1 : 1, and 2 : 1). Total volume of the mixture was maintained at 600 μL. After introducing the API solution and the antisolvent, the vial was sealed by wrapping PARAFILM around the cap of the glass vial. The solutions prepared in the vials were mixed *via* vortex followed by sonication for 5 minutes (Branson 2510). The vials were then observed for solid formation *via* optical microscopy and the resulting solid forms were analyzed *via* Raman spectroscopy.

Cocrystal screening. Cocrystal formation of theophylline and carbamazepine was executed in glass vials to obtain reference solids for comparison with on-chip crystallization results. The off-chip experiments were conducted in 1 mL glass vials (Kimble/Chase). First, solutions of carbamazepine in acetonitrile and theophylline in 1 : 1 chloroform : ethanol were prepared. Subsequently, the CCF solutions were prepared in either acetonitrile (for carbamazepine) or 1 : 1 chloroform : ethanol (for theophylline) at a molar concentration that ensured 1 : 1.2 molar ratio of API : CCF when mixing 400 μL of API solution with 200 μL of CCF solution. 400 μL of API solution was mixed with 200 μL of CCF solution to maintain the 2 : 1 volumetric ratio of the API and CCF chambers on-chip. The solutions prepared in the vials were mixed *via* vortex followed by sonication for 5 minutes (Branson 2510). Each vial was then covered with parafilm (PARAFILM® M) then a small hole was poked in the parafilm so solvent could slowly evaporate (in the range of 4–48 μL h^{-1}). The vials were then monitored for solid form formation and solvent evaporation over a period of 2–48

hours. After complete evaporation of the solvent from the glass vial, the solid form crystallized in each vial was analyzed using optical microscopy (bright field as well as dark field) and Raman spectroscopy.

Results and discussion

Chip design, fabrication and operation

Design of antisolvent addition platform. The 72-well microfluidic platform used here (Fig. 1) is an adaptation of a design we reported previously.[40] Briefly, each of the 8 × 9 wells is comprised of two adjacent chambers for an API solution and an antisolvent respectively (Fig. 1b). The well dimensions of the chambers were varied to screen different volumetric ratios of the two solutions. Each well has a height of 50 μm, a width of 1 mm, and a total length of 2 mm, resulting in total well volumes of approximately 100 nL (combined volume of the two chambers, Fig. 1). The 'lengths' of the two compartments within each well are varied along each row of wells such that API to antisolvent solution ratios (L_{AS}-to-L_{API}) are 2 : 1, 1 : 1, and 1 : 2. Each ratio is replicated 3 times. Varying the relative size of the API and antisolvent solution chambers, as expressed in the length of the chambers (L_{AS} and L_{API}), changes the level of supersaturation achieved upon mixing of different amounts of solvent and antisolvent. Another deviation compared to the previously reported design[40] is that the microchannels connecting adjacent chambers along each row of wells were designed to 'zig-zag' to reduce issues with dead volume and bubbles, ensuring faster and complete filling of large chambers (Fig. 1). More detailed schematics of the platform are provided in the ESI.†

Design of evaporation platform. The microfluidic platform reported here has 24 wells, each comprising of an API chamber, a CCF chamber, and an evaporation chamber (Fig. 1). Each well is isolated from the rest of the wells using a series of normally closed valves.[75,76] This platform can be used for to screen APIs combinatorially with 24 unique conditions: 1 API solution × 6 cocrystal former (CCF) solutions × 4 different possible evaporation rates.

The volume of the API chamber of each well is ~200 nL. When using API solutions at a concentration of 50 mg mL^{-1}, only ~10 μg of API is consumed for each crystallization condition investigated on-chip, two to three orders of magnitude smaller than the quantity of API consumed per condition for a traditional off-chip screening approach (~600 μL per condition).[5,6]

The third chamber, an evaporation chamber, was added to the fluid layer adjacent to each API chamber. The evaporation chamber is connected to the API chamber (containing the mixed API/CCF solutions after mixing) through a separate control valve. The evaporation chamber also is connected to the atmosphere *via* evaporation channels in the EL. Detailed schematics of the evaporation platform as well as details on the rate of solvent evaporation as a function of dimension of the evaporation channels, the parameters affecting the rate of evaporation of solvents through the microchannels, and calculations based on different solvents are provided in the ESI.†

Solvent compatibility of platforms. We enhanced the resistance to solvent absorption of the chip by replacing the PDMS layers with thin layers of SIFEL (total thickness of the SIFEL fluid and control layer ~200 μm). These SIFEL layers were sandwiched between either two 100 μm COC layers, or between a thin layer of COC on top and a thin layer of Teflon FEP at the bottom to minimize transport of the solvents of interest to the outside atmosphere. COC and Teflon FEP are much less permeable to solvents (compared to PDMS and/or SIFEL) and swell less when in contact with solvents.[77] These desirable properties of the materials used for the FLA–IL assembly significantly minimized solvent loss when using organic solvents, including methanol, ethanol, trifluoroethanol, THF, hexane, toluene, and acetonitrile. Depending on the solvent used, the solutions were retained in the chambers on-chip for 2 to more than 12 hours when the wells were isolated from the ambient. Similar to our prior work,[38] an evaporation layer (EL, Fig. 1) is added to the chip enabling evaporative crystallization at designed solvent evaporation rates. This layer is made out of thiolene, a material that is impermeable to air and solvent-vapor, and has superior resistance to a wide range of organic solvents including those mentioned above.[78]

Raman compatibility of platform. Various analytical techniques such as X-ray diffraction (powder and single crystal X-ray), solid state NMR, IR (including near IR and Fourier transform IR) spectroscopy, and Raman spectroscopy are typically used to identify the crystal forms of organic molecules.[79–82] Here, we used Raman spectroscopy for on-chip as well as off-chip solid form identification due to its chemical specificity, high throughput, amenability to automation, and high spatial resolution thus reducing sample needs.[81] Data was acquired following a procedure reported previously.[38] The SIFEL fluid and control layer assembly that is sandwiched between thin COC and Teflon FEP layers (the FLA–IL assembly), is sufficiently transparent to yield signal to noise ratios that permit analysis of solid forms using Raman spectroscopy. Only the non-Raman-transparent EL needs to be removed for spectroscopic analysis. Details, including Raman spectra, regarding background correction of on-chip Raman data are provided in the ESI (Fig. S4†).

Evaporation platform operation. Fluidic routing and mixing on-chip is achieved using an array of normally closed valves (three to five sets) incorporated in the control layer (Fig. 1).[75,83] The API solutions were introduced along the rows into the API and CCF chambers upon actuation of the valve sets labelled "1" and "3" *via* application of vacuum at the control line inlets and at the fluid outlets (Fig. 1b). Next, valve sets 1 and 3 are closed and upon actuating valve set 2 and applying vacuum at the corresponding outlets the CCF chambers are emptied. Next these chambers are purged with API solvent and CCF solutions are introduced. Valve set 2 is then closed to isolate the API and CCF solutions in adjacent chambers. The solutions were mixed by diffusion for approximately an hour by continuous actuation of valve set 3. Valve set 4 was actuated occasionally to push the solutions back and forth between the chambers to achieve better mixing (Fig. 1b). After the solutions were fully mixed, all peripheral connections except the pneumatic tubing to actuate valve set 5 was removed, and the chip was sealed with Crystal Clear Tape to prevent solvent evaporation through the inlets and outlets. Upon actuation of valve set 5 (Fig. 1b), the mixed solutions in the API chamber were exposed to the ambient

through the evaporation channels in the EL to allow for solvent evaporation at designed rates. After completion of the experiment, valve set 5 was closed by releasing the vacuum, thereby isolating the API chambers, cocrystal chambers, evaporation chambers, and the feed lines. The chip was disconnected from the only remaining tubing, enabling easy handling and transport to solid form analysis stations (*i.e.*, optical microscope and Raman microscope).[41,76]

Antisolvent platform operation. The API and antisolvent solutions were introduced by actuation of valve sets "1" and "2" *via* application of vacuum at the control line inlets and application of vacuum at the fluid outlets (Fig. 1b). Next, valve sets 1 and 2 were closed and valve set 3 was actuated for 15–20 minutes to allow diffusional mixing. The now completely filled chip was sealed with Crystal Clear Tape (Hampton Research HR4-511) to prevent solvent evaporation from the inlets and outlets, and placed in a plastic Petri dish along with 2 microcentrifuge tubes filled with the solvent(s) used in the crystallization experiment. The Petri dish was sealed with parafilm to ensure a solvent saturated environment, further minimizing loss of solvent vapor. The Petri-dish with loaded evaporation platform was incubated at room temperature for several hours.

Solvent evaporation rates. Solvent evaporation was quantified as a function of time for different solvents: methanol, ethanol, and acetonitrile by tracing the area covered by the solvent in the microfluidic crystallization well using the "free-hand selection" tool in ImageJ 1.46. For different solvents, the evaporation channel dimensions were redesigned to result in specific evaporation rates based on their volatility, which was indicated by a defined factor K' (see ESI† for details, higher K' values indicates solvent has higher volatility). For methanol and ethanol (evaporation channel dimensions were used corresponding to $K' = 6$ in the ESI†) and for acetonitrile (evaporation channel dimensions were used corresponding to $K' = 15$). Typically, the solvent evaporation rate was controlled by the dimensions of the evaporation channels in the EL and the properties of the solvents. Fig. 3a shows a comparison between the solvent evaporation rates (in percentage volume of the solvent) for methanol employing the solvent resistant microfluidic platforms reported in this study and the previously reported PDMS-based evaporative crystallization platform reported with the same design for the evaporation channels.[38] The observed solvent loss was due to a combination of solvent loss resulting from the chip material (permeation and absorption) and evaporation through the microchannels in the EL connecting the liquid in the well to the ambient.

The PDMS-based evaporation platforms reported previously controlled the evaporation rate of methanol at rates from 7 to 16 nL h^{-1}. The control experiment (with closed evaporation channel) resulted in an evaporation rate of ~4 nL h^{-1}, which is due to the absorption of solvent into PDMS. The absorption of methanol prohibits the application of the platform in the experiments requiring slower solvent evaporation. Comparing to the PDMS-based platform, SIFEL-based evaporative crystallization platforms absorbs less solvent, which enables methanol to evaporate at lower rate, *i.e.* 3.3 nL h^{-1}. The better solvent compatibility of the SIFEL-based platforms also resulted in a better controlled solvent evaporation rates (smaller error bars), thus, more reliable solvent evaporation crystallization results.

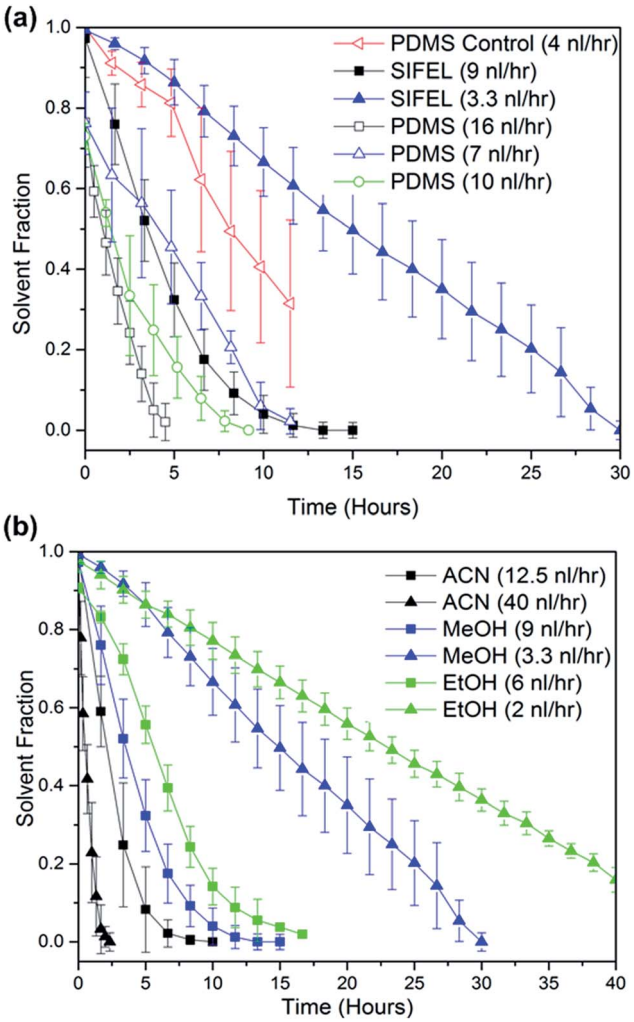

Fig. 3 (a) Comparison of solvent evaporation rates for methanol in PDMS-based and SIFEL-based microfluidic platforms. (b) Solvent evaporation rates for three different solvents in SIFEL-based microfluidic platform: ACN (acetonitrile), MeOH (methanol) and EtOH (ethanol).

Fig. 3b shows a comparison of the solvent evaporation rates for different solvents including methanol, ethanol, and acetonitrile obtained employing the SIFEL-based evaporative crystallization platform. The rates of evaporation for these solvents are: 2 to 8 nL h^{-1} for ethanol and 3.3–9 nL h^{-1} for methanol with minimal well to well variation, and ~12.5 to ~40 nL h^{-1} for acetonitrile. For the lowest solvent evaporation rates (~2 nL h^{-1}) some solvent absorption into the SIFEL-based platform was observed resulting in deviation of the evaporation rates from the designed evaporation rates. We did not observe solvent evaporation for methanol in the control experiment with SIFEL-based evaporation chip (data not shown in Fig. 3). It is acknowledged that many other parameters, such as the location of the through holes in the evaporation chamber, and the size of the hole may affect the rate of solvent loss during the

experiment. Nevertheless, the SIFEL-based microfluidic evaporation platforms provide good control over the evaporation rates, with only 10–20% variation in evaporation rates from well-to-well.

Cocrystal screening experiments (evaporation)

Theophylline and carbamazepine, two commercially available drugs, were used for demonstrating the utility of the platforms for on-chip cocrystal screening. Cocrystals of both APIs with two or three CCFs were screened using the evaporation platform. For theophylline, a chloroform : ethanol (volumetric ratio = 1 : 1) solution of the drug (0.5 M) was introduced along the different rows of wells, with each row corresponding to a different evaporation rate. Chloroform : ethanol (volumetric ratio = 1 : 1) solutions of four acids (malonic, 2,4-dihydroxy benzoic acid, benzoic acid and glutaric acids, 1.2 M each) were introduced along the columns of these wells. Similarly, for carbamazepine, acetonitrile solutions of the drug (0.14 M), were introduced along the rows and acetonitrile solutions of two acids (malic acid and 4-hydroxy benzoic acid, 0.3 M) were introduced along the columns. These solutions were mixed on-chip by diffusion.

No solid formation was observed in about one hour after the mixing of the API and CCF solutions started on-chip. The same solution mixtures prepared off-chip in 1 mL glass vials also did not exhibit solid forms in 24 hours. These observations suggested that the solution mixture was under-saturated with respect to each of the cocrystal forming component and the intended cocrystal.

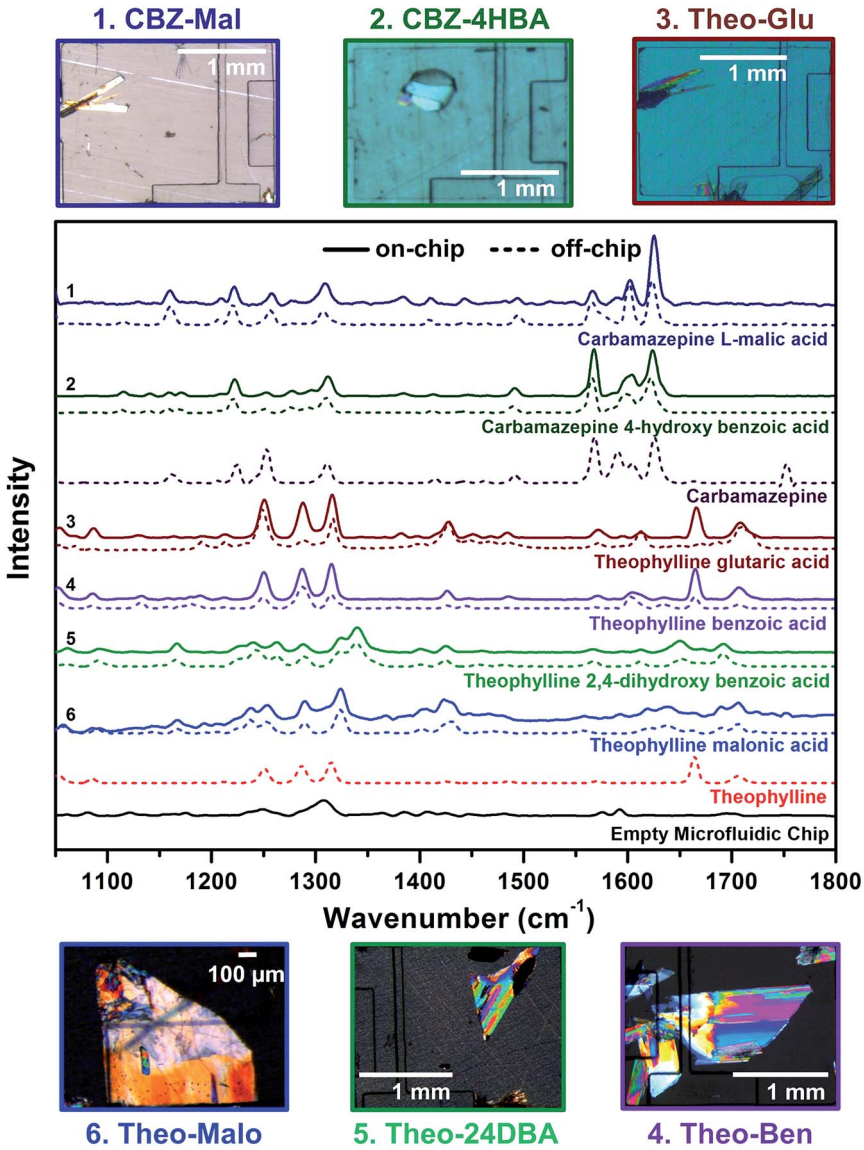

Fig. 4 Magnified views of the high quality cocrystals of carbamazepine and theophylline crystallized on-chip. Raman spectra of carbamazepine and theophylline as well as different carbamazepine and theophylline cocrystals grown and analyzed on-chip (solid lines) and off-chip (dotted lines). The views of the 1050–1800 cm^{-1} range are provided to highlight the lack or presence of spectral differences between the different cocrystals and/or samples grown on-chip and off-chip. "Empty Microfluidic Chip" corresponds to the Raman spectrum of the FLA–IL assembly by itself.

After complete mixing of the solutions on-chip (typically solutions are thoroughly mixed within an hour of valve opening), the solutions were concentrated by solvent evaporation through the microchannels in the EL. For the theophylline screening experiments, the solvent evaporated at a rate of ~20 to 50 nL h^{-1} due to the high volatility of chloroform. For the carbamazepine screening experiments, acetonitrile evaporated at a rate of 12.5 to 40 nL h^{-1}. These controlled evaporation resulted in formation of single crystals of the cocrystals at some of the conditions screened, *e.g.*, carbamazepine–4-hydroxybenzoic acid, theophylline–malonic acid, and theophylline–2,4-dihydroxybenzoic acid (Fig. 4). Aggregation or precipitation of non-crystalline solid was frequently observed in the crystallization chambers with high evaporation rates, whereas single crystals or a few relatively large crystals formed at low evaporation rates. Fig. 4 shows representative images of the cocrystals formed on-chip.

Performing comparable off-chip crystallization experiments in ~600 μL solvent in open vials (high solvent evaporation rates) only resulted in precipitates, gels or agglomerates of the solid forms. Covering the vials with parafilm with 2–5 mm holes significantly slowed down the evaporation and improved the success rate of the crystallization. However, greater number of trials (requiring much more sample) had to be conducted off-chip before high quality and segregated crystals could be obtained. The SIFEL-based microfluidic evaporation platforms allowed the solutions to reach varying supersaturation levels at a controlled rate, which significantly improved the crystallinity of the solid forms obtained.

The solids crystallized on-chip were characterized using Raman spectroscopy on-chip over the range of 1050–1800 cm^{-1} (Fig. 4). For reference, Raman spectra of an empty FLA–IL assembly (Fig. S3†), pure CCFs, pure APIs, and the solid forms crystallized off-chip were collected. The raw data from on-chip experiments was corrected for background from the FLA–IL assembly. An example of the data correction process is provided for the solid form of theophylline and malonic acid in the ESI (Fig. S4†). The Raman spectra of the crystalline solids formed on-chip were in agreement with the reference Raman spectra from the cocrystals obtained in off-chip experiments.

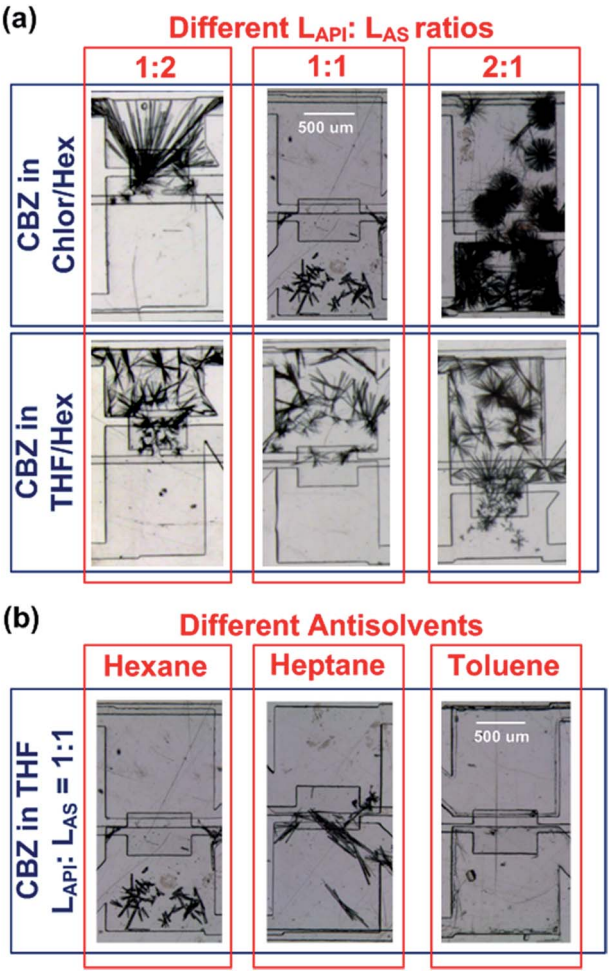

Fig. 5 Magnified views of the microfluidic crystallization wells showing the (a) effect of the ratio of mixing of solvent/antisolvent (L_{API} : L_{AS}) on-chip on crystal habit (shape and number) of carbamazepine and (b) effect of different antisolvents on polymorph of carbamazepine crystallized on chip.

Polymorph screening experiments (antisolvent addition)

Polymorph screening of carbamazepine was used to validate the antisolvent addition platform. Carbamazepine solutions in THF and chloroform were mixed with different antisolvents (hexane, toluene and heptane) on-chip where the volumetric ratio of L_{API} : L_{AS} was varied (2 : 1, 1 : 1, and 1 : 2). The solutions were then mixed on-chip. The nature of the solid forms varied upon changing the ratio of solvent to antisolvent (Fig. 5a). In experiments performed at high supersaturation, very fine and numerous crystals were obtained, whereas fewer and larger crystals were obtained in experiments performed at lower supersaturation. When carbamazepine in chloroform was crystallized with hexane as the antisolvent very thin and dense solid forms were obtained at higher supersaturation while thick, long plate-like crystal aggregates were obtained at lower supersaturation. Similar off-chip experiments for different ratios of solvent and antisolvent resulted in rapid precipitation due to convective mixing compared to diffusional mixing of the solutions on-chip. Similar trends were observed for mixing at high and low levels of supersaturation, however, in off-chip experiments typically mixture of thin, dense and thick, long plate-like forms were observed.

In separate experiments, we observed that use of different antisolvents resulted in crystallization of different polymorphs of carbamazepine (Fig. 5b). When THF is used as the solvent in combination with hexane or heptane as the antisolvent, long needles (polymorph form II, *vide infra*) were obtained, whereas prismatic crystals (form III) were obtained in combination with toluene as the antisolvent. In similar off-chip experiments for different antisolvents, we were not able to distinguish between the solid forms for formation of different polymorphs. This may be attributed primarily to the formation of polymorph form II on relatively rapid mixing of solutions, which made identification of polymorph form III (if formed) challenging. Through

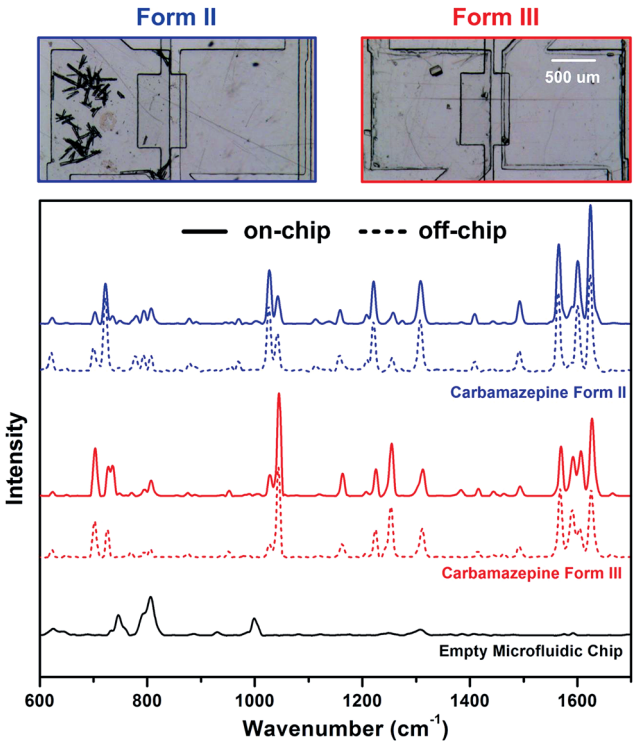

Fig. 6 Magnified views of high quality crystals of different polymorph forms of carbamazepine crystallized on-chip. Raman spectra of different polymorphs of carbamazepine grown and analyzed on-chip (solid lines) and off-chip (dotted lines). The views of the 600–1700 cm^{-1} range are provided to highlight the lack or presence of spectral differences between the different salts and/or samples grown on-chip and off-chip. "Empty Microfluidic chip" corresponds to the Raman spectrum of the FLA-substrate assembly by itself.

these experiments we are able to demonstrate the compatibility of the SIFEL-based antisolvent chip with a variety of solvents (water and non-polar solvents).

The solid forms were distinguished *via* on-chip Raman spectroscopy, comparing Raman spectra for the two polymorphs crystallized on-chip and off-chip in the range of 600–1700 cm^{-1} (Fig. 6). The on-chip Raman spectra were in good agreement with the Raman spectra for the polymorphs obtained in off-chip experiments.

Conclusions

We have developed and validated a hybrid COC–SIFEL–PDMS–Teflon–thiolene based microfluidic platform for cocrystal and polymorph screening of APIs at sub-μL scale. As in previous renditions, these microfluidic platforms are comprised of well arrays that enable screening of unique crystallization conditions, but here we drastically enhance compatibility of these chips with strong organic solvents that are typically used in pharmaceutical crystallization including acetonitrile, ethanol, chloroform, and toluene. Furthermore, integration of thin PDMS/SIFEL layers sandwiched between COC and Teflon sheets rendered the chips compatible with on-chip solid form analysis *via* Raman spectroscopy.

Carbamazepine and theophylline were used to validate the capability of the microfluidic chips with respect to their ability to screen and identify multiple cocrystal forms and polymorphs of APIs while using strong organic solvents including ethanol, methanol, THF, acetonitrile, chloroform, hexane, and toluene. Subsequently, we successfully confirmed the identity of the solid forms *via* on-chip Raman spectroscopic analysis.

The hybrid COC–SIFEL–PDMS–Teflon–thiolene based microfluidic platforms exhibit minimal solvent loss due to solvent absorption by the chip materials, thus eliminating issues with swelling, gradual dry-out, and associated changes in concentrations. This drastically increases the likelihood of reproducible crystallization of single, isolated crystals on-chip, even when using strong organic solvents. Moreover, the antisolvent hybrid chips offer the flexibility to employ several antisolvents on the same chip to screen for different crystal habits and polymorphs. Solvent compatible microfluidic chips such as those reported here will broaden the scope of application of microfluidic platforms for solid form screening with a multitude of solvents, in addition to enabling identification of the solid forms of an API, with optimal physicochemical properties at an early stage in the drug discovery process, at a time when only limited quantities of each API (~10 mg) are available.

Acknowledgements

We would like to thank AbbVie Laboratories for financial support and the National Science Foundation for a Graduate Research Fellowship to EMH (Grant DGE-1144245). Part of this work made use of the facilities in the Micro- & Nanotechnology Laboratory as well as the Frederick Seitz Materials Research Laboratory Central Facilities at University of Illinois at Urbana-Champaign, which is partially supported by the U.S. Department of Energy under grants DE-FG02-07ER46453 and DE-FG02-07ER46471. We thank Dr Amit V. Desai for stimulating discussions.

References

1 N. Rasenack and B. W. Müller, *Int. J. Pharm.*, 2002, **244**, 45–57.
2 T. Lee, Y. H. Chen and C. W. Zhang, *Pharm. Technol.*, 2007, **31**, 72–87.
3 G. P. Stahly, *Cryst. Growth Des.*, 2007, **7**, 1007–1026.
4 C. R. Gardner, C. T. Walsh and O. Almarsson, *Nat. Rev. Drug Discovery*, 2004, **3**, 926–934.
5 L. Kumar, A. Amin and A. K. Bansal, *Drug Discovery Today*, 2007, **12**, 1046–1053.
6 C. R. Gardner, O. Almarsson, H. Chen, S. Morissette, M. Peterson, Z. Zhang, S. Wang, A. Lemmo, J. Gonzalez-Zugasti, J. Monagle, J. Marchionna, S. Ellis, C. McNulty, A. Johnson, D. Levinson and M. Cima, *Comput. Chem. Eng.*, 2004, **28**, 943–953.
7 G. Charvin, F. R. Cross and E. D. Siggia, *PLoS One*, 2008, **3**, e1468.
8 N. Q. Balaban, J. Merrin, R. Chait, L. Kowalik and S. Leibler, *Science*, 2004, **305**, 1622–1625.

9 E. A. Ottesen, J. W. Hong, S. R. Quake and J. R. Leadbetter, *Science*, 2006, **314**, 1464–1467.
10 R. G. Blazej, P. Kumaresan and R. A. Mathies, *Proc. Natl. Acad. Sci. U. S. A.*, 2006, **103**, 7240–7245.
11 W. H. Grover, A. M. Skelley, C. N. Liu, E. T. Lagally and R. A. Mathies, *Sens. Actuators, B*, 2003, **89**, 315–323.
12 T. D. Wheeler, D. Zeng, A. V. Desai, B. Onal, D. E. Reichert and P. J. A. Kenis, *Lab Chip*, 2010, **10**, 3387–3396.
13 R. Sista, Z. Hua, P. Thwar, A. Sudarsan, V. Srinivasan, A. Eckhardt, M. Pollack and V. Pamula, *Lab Chip*, 2008, **8**, 2091–2104.
14 R. J. Meagher, A. V. Hatch, R. F. Renzi and A. K. Singh, *Lab Chip*, 2008, **8**, 2046–2053.
15 S. Guha, S. L. Perry, A. Pawate and P. J. A. Kenis, *Sens. Actuators, B*, 2012, **174**, 1–9.
16 S. L. Perry, G. W. Roberts, J. D. Tice, R. B. Gennis and P. J. A. Kenis, *Cryst. Growth Des.*, 2009, **9**, 2566–2569.
17 S. Talreja and M. S. Thesis, *Elucidation of Protein-Precipitant Phase Diagrams and Their Link to Crystal Quality*, University of Illinois at Urbana-Champaign, 2005.
18 S. Talreja, D. Y. Kim, A. Y. Mirarefi, C. F. Zukoski and P. J. A. Kenis, *J. Appl. Crystallogr.*, 2005, **38**, 988–995.
19 S. Talreja, S. L. Perry, S. Guha, V. Bhamidi, C. F. Zukoski and P. J. A. Kenis, *J. Phys. Chem. B*, 2010, **114**, 4432–4441.
20 S. Selimovic, F. Gobeaux and S. Fraden, *Lab Chip*, 2010, **10**, 1696–1699.
21 J. Shim, G. Cristobal, D. R. Link, T. Thorsen and S. Fraden, *Cryst. Growth Des.*, 2007, **7**, 2192–2194.
22 W. Du, L. Li, K. P. Nichols and R. F. Ismagilov, *Lab Chip*, 2009, **9**, 2286–2292.
23 L. Li, W. Du and R. F. Ismagilov, *J. Am. Chem. Soc.*, 2009, **132**, 112–119.
24 L. Li and R. F. Ismagilov, *Annu. Rev. Biophys.*, 2010, **39**, 139–158.
25 B. Zheng, L. S. Roach and R. F. Ismagilov, *J. Am. Chem. Soc.*, 2003, **125**, 11170–11171.
26 B. Zheng, J. D. Tice, L. S. Roach and R. F. Ismagilov, *Angew. Chem., Int. Ed.*, 2004, **43**, 2508–2511.
27 C. Hansen and S. R. Quake, *Curr. Opin. Struct. Biol.*, 2003, **13**, 538–544.
28 C. L. Hansen, S. Classen, J. M. Berger and S. R. Quake, *J. Am. Chem. Soc.*, 2006, **128**, 3142–3143.
29 C. L. Hansen, E. Skordalakes, J. M. Berger and S. R. Quake, *Proc. Natl. Acad. Sci. U. S. A.*, 2002, **99**, 16531–16536.
30 C. J. Gerdts, V. Tereshko, M. K. Yadav, I. Dementieva, F. Collart, A. Joachimiak, R. C. Stevens, P. Kuhn, A. Kossiakoff and R. F. Ismagilov, *Angew. Chem., Int. Ed.*, 2006, **45**, 8156–8160.
31 B. Zheng, J. D. Tice and R. F. Ismagilov, *Adv. Mater.*, 2004, **16**, 1365–1368.
32 C. L. Hansen, E. Skordalakes, J. M. Berger and S. R. Quake, *Proc. Natl. Acad. Sci. U. S. A.*, 2002, **99**, 16531–16536.
33 B. Zheng, C. J. Gerdts and R. F. Ismagilov, *Curr. Opin. Struct. Biol.*, 2005, **15**, 548–555.
34 P. Laval, J. B. Salmon and M. Joanicot, *J. Cryst. Growth*, 2007, **303**, 622–628.
35 M. Ildefonso, N. Candoni and S. Veesler, *Org. Process Res. Dev.*, 2012, **16**, 556–560.
36 A. Feuerborn, A. Prastowo, P. R. Cook and E. Walsh, *Lab Chip*, 2015, **15**, 3766–3775.
37 B. Zheng, J. D. Tice, L. S. Roach and R. F. Ismagilov, *Angew. Chem., Int. Ed. Engl.*, 2004, **43**, 2508–2511.
38 S. Goyal, M. R. Thorson, C. L. Schneider, G. G. Z. Zhang, Y. Gong and P. J. A. Kenis, *Lab Chip*, 2013, **13**, 1708–1723.
39 L. Li, W. Du and R. F. Ismagilov, *J. Am. Chem. Soc.*, 2010, **132**(1), 112–119.
40 M. R. Thorson, S. Goyal, Y. Gong, G. G. Z. Zhang and P. J. A. Kenis, *CrystEngComm*, 2012, **14**, 2404–2412.
41 M. R. Thorson, S. Goyal, B. R. Schudel, C. F. Zukoski, G. G. Z. Zhang, Y. Gong and P. J. A. Kenis, *Lab Chip*, 2011, **11**, 3829–3837.
42 S. Goyal, M. R. Thorson, G. G. Z. Zhang, Y. Gong and P. J. A. Kenis, *Cryst. Growth Des.*, 2012, **12**, 6023–6034.
43 P. Laval, A. Crombez and J.-B. Salmon, *Langmuir*, 2008, **25**, 1836–1841.
44 P. Laval, N. Lisai, J. B. Salmon and M. Joanicot, *Lab Chip*, 2007, **7**, 829–834.
45 M. Ildefonso, E. Revalor, P. Punniam, J. B. Salmon, N. Candoni and S. Veesler, *J. Cryst. Growth*, 2012, **342**, 9–12.
46 A. Y. Lee, I. S. Lee, S. S. Dette, J. Boerner and A. S. Myerson, *J. Am. Chem. Soc.*, 2005, **127**, 14982–14983.
47 E. M. Horstman, J. A. Bertke, E. H. Kim, L. C. Gonzalez, G. G. Z. Zhang, Y. Gong and P. J. A. Kenis, *CrystEngComm*, 2015, **17**, 5299–5306.
48 K. Dhouib, C. Khan Malek, W. Pfleging, B. Gauthier-Manuel, R. Duffait, G. Thuillier, R. Ferrigno, L. Jacquamet, J. Ohana, J.-L. Ferrer, A. Theobald-Dietrich, R. Giege, B. Lorber and C. Sauter, *Lab Chip*, 2009, **9**, 1412–1421.
49 G. Kisselman, W. Qiu, V. Romanov, C. M. Thompson, R. Lam, K. P. Battaile, E. F. Pai and N. Y. Chirgadze, *Acta Crystallogr., Sect. D: Biol. Crystallogr.*, 2011, **67**, 533–539.
50 J. D. Ng, P. J. Clark, R. C. Stevens and P. Kuhn, *Acta Crystallogr., Sect. D: Biol. Crystallogr.*, 2008, **64**, 189–197.
51 J.-U. Shim, S. N. Patil, J. T. Hodgkinson, S. D. Bowden, D. R. Spring, M. Welch, W. T. S. Huck, F. Hollfelder and C. Abell, *Lab Chip*, 2011, **11**, 1132–1137.
52 E. M. Horstman, S. Goyal, A. Pawate, G. Lee, G. G. Z. Zhang, Y. Gong and P. J. A. Kenis, *Cryst. Growth Des.*, 2015, **15**, 1201–1209.
53 K. T. Savjani, A. K. Gajjar and J. K. Savjani, *ISRN Pharm.*, 2012, **2012**, 195727.
54 J. N. Lee, C. Park and G. M. Whitesides, *Anal. Chem.*, 2003, **75**, 6544–6554.
55 R. R. Lamonte and D. McNally, *Adv. Mater. Processes*, 2001, **159**, 33–36.
56 D. Bartolo, G. Degre, P. Nghe and V. Studer, *Lab Chip*, 2008, **8**, 274–279.
57 C. Harrison, J. Cabral, T. C. M. Stafford, A. Karim and E. J. Amis, *J. Micromech. Microeng.*, 2004, **14**, 153–158.
58 L. H. Hung, R. Lin and A. P. Lee, *Lab Chip*, 2008, **8**, 983–987.
59 A. Taberham, M. Kraft, M. Mowlem and H. Morgan, *J. Micromech. Microeng.*, 2008, **18**, 064011.

60 J. P. Rolland, E. C. Hagberg, G. M. Denison, K. R. Carter and J. M. De Simone, *Angew. Chem., Int. Ed.*, 2004, **43**, 5796–5799.
61 J. P. Rolland, R. M. Van Dam, D. A. Schorzman, S. R. Quake and J. M. DeSimone, *J. Am. Chem. Soc.*, 2004, **126**, 2322–2323.
62 T. J. A. Renckens, D. Janeliunas, H. van Vliet, J. H. van Esch, G. Mul and M. T. Kreutzer, *Lab Chip*, 2011, **11**, 2035–2038.
63 N. S. G. K. Devaraju and M. A. Unger, *Lab Chip*, 2011, **11**, 1962–1967.
64 K. Ren, W. Dai, J. Zhou, J. Su and H. Wu, *Proc. Natl. Acad. Sci. U. S. A.*, 2011, **108**, 8162–8166.
65 G. S. Fiorini, M. Yim, G. D. M. Jeffries, P. G. Schiro, S. A. Mutch, R. M. Lorenz and D. T. Chiu, *Lab Chip*, 2007, **7**, 923–926.
66 E. Roy, J.-C. Galas and T. Veres, *Lab Chip*, 2011, **11**, 3193–3196.
67 J. Steigert, S. Haeberle, T. Brenner, C. Muller, C. P. Steinert, P. Koltay, N. Gottschlich, H. Reinecke, J. Ruhe, R. Zengerle and J. Ducree, *J. Micromech. Microeng.*, 2007, **17**, 333–341.
68 G. Sharma, L. Klintberg and K. Hjort, *J. Micromech. Microeng.*, 2011, **21**, 025016.
69 H. Sato, H. Matsumura, S. Keino and S. Shoji, *J. Micromech. Microeng.*, 2006, **16**, 2318–2322.
70 H.-S. Noha, Y. Huangb and P. J. Hesketha, *Sens. Actuators, B*, 2004, **102**, 78–85.
71 S. Metz, R. Holzer and P. Renaud, *Lab Chip*, 2001, **1**, 29–34.
72 A. Asthana, Y. Asthana, I.-K. Sung and D.-P. Kim, *Lab Chip*, 2006, **6**, 1200–1204.
73 S. Begolo, G. Colas, J.-L. Viovy and L. Malaquin, *Lab Chip*, 2011, **11**, 508–512.
74 S. L. Childs, G. P. Stahly and A. Park, *Mol. Pharmaceutics*, 2007, **4**, 323–338.
75 B. R. Schudel, C. J. Choi, B. T. Cunningham and P. J. A. Kenis, *Lab Chip*, 2009, **9**, 1676–1680.
76 R. Mohan, B. R. Schudel, A. V. Desai, J. D. Yearsley, C. A. Apblett and P. J. A. Kenis, *Sens. Actuators, B*, 2011, **160**, 1216–1223.
77 P. S. Nunes, P. D. Ohlsson, O. Ordeig and J. P. Kutter, *Microfluid. Nanofluid.*, 2010, **9**, 145–161.
78 Z. T. Cygan, J. T. Cabral, K. L. Beers and E. J. Amis, *Langmuir*, 2005, **21**, 3629–3634.
79 M. Allesø, S. Velaga, A. Alhalaweh, C. Cornett, M. A. Rasmussen, F. Van Der Berg, H. L. d. Diego and J. Rantanen, *Anal. Chem.*, 2008, **80**, 7755–7764.
80 F. G. Vogt, J. S. Clawson, M. Strohmeier, A. J. Edwards, T. N. Pham and S. A. Watson, *Cryst. Growth Des.*, 2008, **9**, 921–937.
81 T. Kojima, S. Onoue, N. Murase, F. Katoh, T. Mano and Y. Matsuda, *Pharm. Res.*, 2006, **23**, 806–812.
82 Y. Meng, D. J. Weidner, G. D. Gwanmesia, R. C. Liebermann, M. T. Vaughan, Y. Wang, K. Leinenweber, R. E. Pacalo, A. Yeganeh-Haeri and Y. Zhao, *J. Geophys. Res.*, 1993, **98**, 22199–22207.
83 S. Goyal, M. R. Thorson, Y. Gong, G. G. Z. Zhang and P. J. A. Kenis, *Cryst. Growth Des.*, 2012, **12**, 6023–6034.